Microfabricated Platform for Studying Stem Cell Fates

Vicki I. Chin,[1] Philippe Taupin,[2]* Sandeep Sanga,[1] John Scheel,[2] Fred H. Gage,[2] Sangeeta N. Bhatia[1]

[1]Departments of Bioengineering & Medicine, 9500 Gilman Dr. MC, University of California, San Diego, La Jolla, California 92093-0412; telephone: (858) 822-3142; fax: (858) 822-4203; e-mail: sbhatia@ucsd.edu
[2]Laboratory of Genetics, The Salk Institute, La Jolla, California

Received 2 February 2004; accepted 11 June 2004

Published online 12 October 2004 in Wiley InterScience (www.interscience.wiley.com). DOI: 10.1002/bit.20254

Abstract: Platforms that allow parallel, quantitative analysis of single cells will be integral to realizing the potential of postgenomic biology. In stem cell biology, the study of clonal stem cells in multiwell formats is currently both inefficient and time-consuming. Thus, to investigate low-frequency events of interest, large sample sizes must be interrogated. We report a simple, versatile, and efficient micropatterned arraying system conducive to the culture and dynamic monitoring of stem cell proliferation. This platform enables: 1) parallel, automated, long-term (~days to weeks), live-cell microscopy of single cells in culture; 2) tracking of individual cell fates over time (proliferation, apoptosis); and 3) correlation of differentiated progeny with founder clones. To achieve these goals, we used microfabrication techniques to create an array of ~10,000 microwells on a glass coverslip. The dimensions of the wells are tunable, ranging from 20 to >500 μm in diameter and 10–500 μm in height. The microarray can be coated with adhesive proteins and is integrated into a culture chamber that permits rapid (~min), addressable monitoring of each well using a standard programmable microscope stage. All cells share the same media (including paracrine survival signals), as opposed to cells in multiwell formats. The incorporation of a coverslip as a substrate also renders the platform compatible with conventional, high-magnification light and fluorescent microscopy. We validated this approach by analyzing the proliferation dynamics of a heterogeneous adult rat neural stem cell population. Using this platform, one can further interrogate the response of distinct stem cell subpopulations to microenvironmental cues (mitogens, cell–cell interactions, and cell–extracellular matrix interactions) that govern their behavior. In the future, the platform may also be adapted for the study of other cell types by tailoring the surface coatings, microwell dimensions, and culture environment, thereby enabling parallel investigation of many distinct cellular responses.

Keywords: stem cells; clonal assay; BioMEMS; microfabrication; high-throughput

Correspondence to: Sangeeta N. Bhatia

*Present address: National Neuroscience Institute, Singapore 308433, Republic of Singapore.

Contract grant sponsors: the La Jolla Interfaces in Science, Burroughs Wellcome Fund (to V.I.C.), the David and Lucile Packard Foundation (to S.N.B.)

INTRODUCTION

Cell-based assays have long been used in stem cell research to understand basic mechanisms of cellular fate and function. In stem cell studies, clonal and single cell assays are essential for determining self-renewal potential (Nakauchi et al., 2001) and identifying regulators of stem cell proliferation and differentiation (Lemischka, 1999). Currently, the tools available to study the role of the cellular microenvironment on cell fate processes are relatively limited—in part, due to the number of interdependent variables (soluble factors, cell–cell interactions, cell–matrix interactions). Investigation of these variables using conventional cell-based assays can be prohibitive in terms of materials, space, and time. Current techniques for single cell counting and sorting include flow cytometry and fluorescence activated cell sorting (FACS) technologies (Orfao and Ruiz-Arguelles, 1996). The instruments are capable of screening up to 50,000 cells/sec, but once interrogated the cells are usually lost within a bulk population. Single cells may be sorted into 96-well plates for further culture in some FACS systems, but manual tracking of the cell fate of large numbers of individual cells and their behavior over time remains cumbersome. The development of miniaturized platforms for cell-based assays may provide a simple and efficient alternative for conducting long-term, parallel studies of stem cell fate. Elsewhere in the biological arena, microfabrication has revolutionized the study of genomics with the development of DNA microarrays (Pease et al., 1994; Wu et al., 2002), RNA microarrays (Seetharaman et al., 2001), and protein arrays (MacBeath and Schreiber, 2000). In this study, we focus on the application of miniaturization technology to enhance the study of stem cell fate.

Current approaches to improve cell-based assays can be categorized by attempts to make assays more: 1) automated, 2) precise, or 3) parallel. In the automation realm, recent work on high-speed automated microscopy has begun to permit single-cell analysis on the subcellular level. On-the-fly autofocus technology enables rapid scans of 96-well plates and whole slides for ultra-rare event detection (Bajaj

et al., 2000; Price et al., 2002). With this system, more than 20×10^6 cells were analyzed for in situ markers of proliferation and apoptosis. Other companies, such as Cellomics (Pittsburgh, PA), have developed algorithms to automate the image analysis associated with cellular processes such as the translocation of fluorescently labeled transcription factors (Blake, 2001). Despite the utility of such highly automated platforms in industry (Palsson et al., 2003), these tools are not typically suitable for long-term, aseptic culture (~ days) and live, single-cell tracking required for stem cell biology applications. In addition to progress in automation, investigators have developed assays to screen cellular responses in arrays on solid substrates (Ziauddin and Sabatini, 2001). Parallel assays that employ spatially encoded arrays have the advantage of rapid identification of a "hit" or promising lead rather than being well suited to the investigation of large numbers of clonal populations. Finally, cell-based assays have been developed that allow one to precisely control and study the role of the cellular microenvironment. In particular, 2D (flat), cellular micropatterns fabricated by selective adhesion of cells to patterned substrates have been utilized to study the role of extracellular matrix in nerve growth cone guidance (Clark et al., 1993; Hammarback et al., 1988), the role of cell shape in regulating cell fate (Chen et al., 1997), and the role of cell–cell interactions in cell cycle control and tissue-specific functions (Bhatia et al., 1999; Nelson and Chen, 2002; Voldman et al., 1999).

While "micropatterning" via selective adhesion is useful for many applications, in fact 2D cellular micropatterns often deteriorate over time (Nelson et al., 2003). To counteract the tendency for micropatterned cells to migrate, 3D microwells have been fabricated from agarose (Nelson et al., 2003), acrylamide, and polydimethylsiloxane (PDMS) (Jackman et al., 1998; Ostuni et al., 2001) in order to confine cells over time. Microwells have also been etched in glass (Inoue et al., 2001), silicon (Parce et al., 1989), and fiber optics (Biran and Walt, 2002; Taylor and Walt, 2000; Walt, 2002). Cells are patterned either by dragging a PDMS block across the surface to force the cells into the wells (You et al., 1997), by gravitational sedimentation (Parce et al., 1989), or by selective deposition of proteins within the wells (Ostuni et al., 2001). These latter studies using microwells have shown proof-of-concept designs using robust organisms, such as bacteria, yeast, and immortalized cell lines, and one challenge facing this area is the application to more delicate cell types, such as specialized, organ-specific mammalian cells and stem cells of various origins.

In this study, we present and characterize a robust, microfabricated platform for the microscopic investigation of adult neural stem cell fates. A high-density array of microwells was integrated into a fluidic chamber to guide deposition of adult neural stem cells and confine their progeny. Adult neural stem cells, found in the subventricular zone (Lois and Alvarez-Buylla, 1993) and the subgranular zone of the dentate gyrus of the hippocampus (Gage et al., 1995b), have the potential to differentiate into a variety of neural cell types in vitro and in vivo (e.g., neurons, glial cells, and oligodendrocytes) (Flax et al., 1998). To exploit their full therapeutic potential, the regulation of proliferation (self-renewal) and differentiation must be better understood. To date, characterization of adult neural stem cells has been confounded by the lack of surface markers for isolation, resulting in a heterogeneous neural progenitor cell (NPC) population in vitro (Ivanova et al., 2002; Suslov et al., 2002). Another experimental challenge has been loss of viability in clonal cultures due to a loss of paracrine signaling unless cultures are rescued with conditioned media containing cystatin C (CCg) (Taupin et al., 2000). As a result of these difficulties, large-scale quantitative studies on the effect of mitogenic factors on cell fate have not been conducted. Certain mitogens, predominantly FGF-2 and EGF, are known to have an effect on the proliferative capacity of neural stem cells (Sommer and Rao, 2002). Other mitogens, such as PDGF (van Heyningen et al., 2001), sonic hedgehog (Shh) (Lai et al., 2003), and neurotrophin-3 (NT-3) (Kalcheim et al., 1992) have an effect on more restricted precursor cells. Using a high-density array platform to screen large numbers of clonal populations may help elucidate the relative role of potential mitogenic factors and their cofactors on true stem cells and more committed progenitors. In this report, we present the design, characterization, and validation of a microfabricated platform for parallel experimental analysis of neural stem cell fates. With this system, we were able to quantitatively track 3,000+ single AHPs for days, obviate the need for conditioned media, and perform high magnification microscopy on differentiated progeny.

MATERIALS AND METHODS

Neural Progenitor Cell Culture

Adult hippocampal progenitor cells (AHPs) were prepared and cultured as described previously (Gage et al., 1995b; Song et al., 2002). For this study, medium to late AHPs (Passage 20–25) that had been infected with a retrovirus to express green fluorescent protein (GFP) (Palmer et al., 1999) were used. Cells were grown on poly-ornithine and laminin-coated tissue culture plates and maintained in DMEM/F12 media supplemented with 2 mM L-glutamine, N2 supplement (Sigma, St. Louis, MO), and 20 ng/mL fibroblast growth factor-2 (FGF-2). To promote neural lineage differentiation, the proliferation media was replaced with DMEM/F12 media with N2 supplement, 2 mM L-glutamine, 0.2 μM retinoic acid (Sigma), and 5 mM forskilin (Sigma). Media were replaced every 4 days.

Microfabrication

Thirty-four mm coverslips (Fisher Scientific, Pittsburgh, PA) were cleaned in sequential washes in acetone, isopropanol, methanol, and deionized (18 MΩ) water and dried under a nitrogen stream. The coverslips were then further cleaned by exposure to oxygen plasma on a Technics 500 II

Asher at a base pressure of 80 mTorr and O_2 pressure of 120 mTorr at a power of 200 W for 10 min.

SU-8 50 or SU-8 100 photoresist (Microchem, Newton, MA), negative photoresists, were statically dispensed and allowed to spread at 500 RPM for 10 sec and ramped to a final spin speed of 2,000 rpm over 30 sec. The photoresist was soft baked for 20 min at 95°C to evaporate the solvent and solidify the film, cooled at room temperature for 10 min, and exposed on a Kasper 2001 Contact Mask Aligner at 365 nm for 60–75 sec, for ~200 mJ/cm^2 total exposure energy through a patterned emulsion mask. Emulsion masks were designed on CorelDraw 11.0 and printed using a Linotronic-Hercules 3300 dpi high-resolution printer. The mask was placed in contact with the SU-8 film and weighted down with a quartz slide. The exposed photoresist was then baked for 2 h at 95°C on a level hot plate, developed in PMacetate, and cured at 200°C for 1 h to complete cross-linking of the remaining film. The final film thickness was verified using a Dektak 3030 profilometer. To ensure the biocompatibility of the SU-8 array, the array was soaked in sterile, distilled water overnight to leach out any residual species from the patterning process. Samples were sterilized by immersion in 70% ethanol in DI water under a UV germicidal lamp for 1 h, rinsed in sterile water 3 times, and stored wet until further use.

Cell Arraying

A Rose tissue culture chamber was modified for flow-based cell arraying (Fig. 1A) (Lodin et al., 1970). Briefly, the chamber is formed by two 34-mm glass coverslips (the bottom coverslip houses the microfabricated wells) sandwiching a 3-mm silicone rubber gasket (Burke Rubber, Monrovia, CA). The bottom coverslip was coated with poly-ornithine and laminin, as previously described (Gage et al., 1995b). The diffusivity of oxygen through the rubber gasket is relatively high and sufficient to sustain most cell types we tested. Two anodized aluminum plates were custom-machined to complete the chamber. To load cells into the chamber, a solution of cells in media was injected through the gasket using an 18-gauge needle and 3-mL syringe while a needle connected to tubing on the opposing side served as the outlet port.

Neural progenitor cells were seeded in the array chamber at a concentration of 17,500, 35,000, or 75,000 cells/mL by injection at 1 mL/sec. Cells were allowed to sediment into underlying wells for 5 min. Subsequent flushing of the chamber with fresh medium removed cells that were not shear-protected in microfabricated wells. The number of washes required to achieve acceptable arraying was empirically determined by microscopic visualization, but

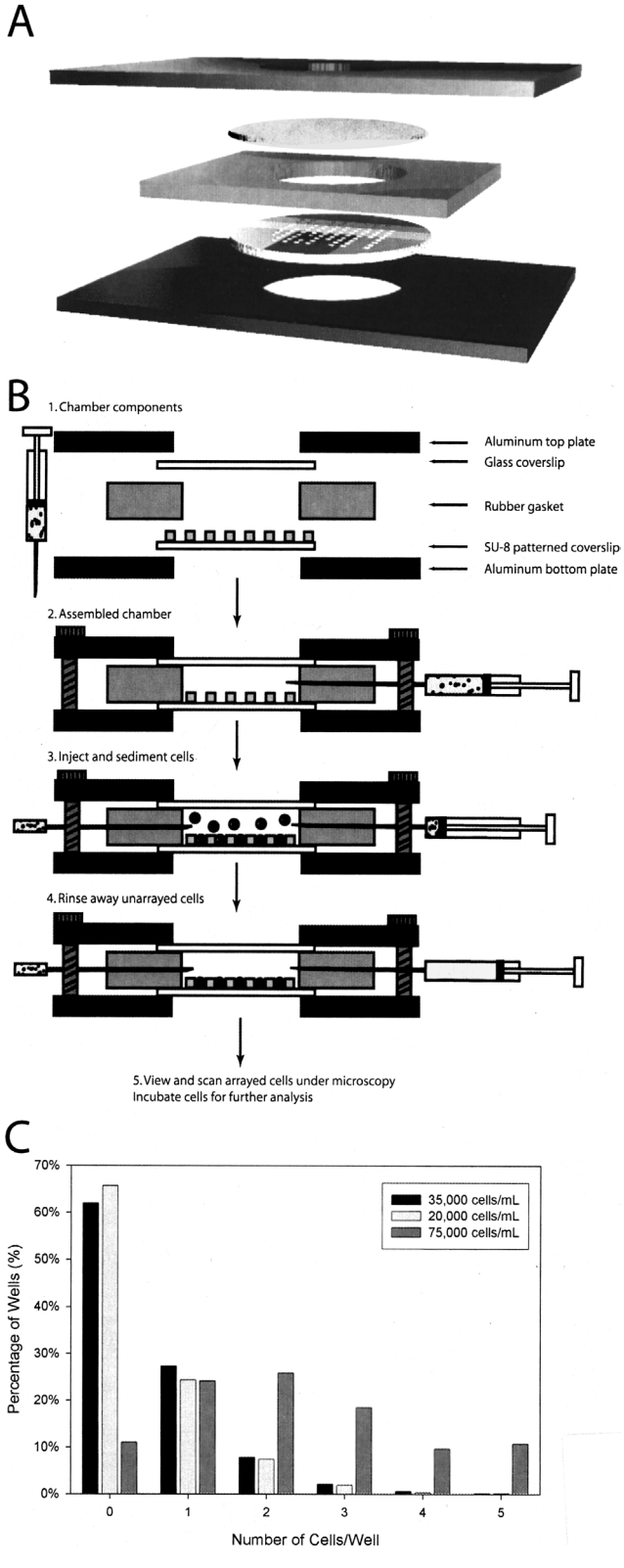

Figure 1. Components and process for creating and assembling the microfabricated chamber. **A:** An exploded 3D view of the components and their assembly order. **B:** A cross-sectional diagram of the assembly and arraying process. After the chamber is assembled, cells are injected through the gasket and allowed to sediment for 3–5 min. After the cells have settled on the surface of the SU-8 patterned coverslip, the cell-seeding medium is completely evacuated and replaced with growth factor enhanced media. The chamber is now ready for analysis via microscopy and further incubation. **C:** The distribution of cell number per well at a cell seeding density of 20,000, 35,000, and 75,000 cells/mL.

generally varied between 1–3 washes of 2 mL. After washing, the chamber was completely filled with culture media and placed in a humidified 37°C, 5% CO_2 incubator. For differentiation studies, cells in the chamber were grown for 4 days in proliferation media and then switched to differentiation media for another 4 days.

Indirect Immunofluorescence

Indirect immunofluorescence was carried out on differentiated cells as previously described (Song et al., 2002; Takahashi et al., 1999). The culture chambers were disassembled and the patterning coverslips were isolated for the immunostaining procedure. Cells were fixed with 4% paraformaldehyde, exposed to primary antibodies (anti beta-tubulin III (Tuj1) (1/5000, Promega, Madison, WI), GFAP (1/2,500, Dako, Carpinteria, CA), and then secondary antibodies (AlexaFluor, Molecular Probes, Eugene, OR). Triton-X (0.05%) was used to stain the intracellular antigens and did not affect the quality of the staining. For visualization of the laminin-coated substrate, the substrate was exposed to an anti-laminin primary (1:40, Biodesign, Kennebunk, ME) and a fluorescent secondary. The samples were visualized by fluorescence microscopy with ex/em 541/565 and ex/em 360/460 nm. All samples were compared to isotype-matched controls.

High-Throughput Microscopy and Analysis

Images of cells within the chamber were acquired on a Nikon Eclipse 3000 equipped with a Ludl MAC 2000 XYZ stage controller. A custom-machined holder ensured that the chamber was fixed in place on the stage during acquisition. Each data acquisition was zeroed to an alignment marker on the coverslip, thus ensuring repeatable data scans. The x–y stage was then programmed to raster across the cell array surface, acquiring images. Thus, a registered scan of the array surface may be acquired at any time in culture. The first time point (day 0) was acquired 5 h after seeding, and subsequent timepoints were acquired 24, 48, and 96 h after seeding. Between scans, the chamber was returned to the incubator. For each time point the same 324 image fields were acquired at 10× magnification in Hoffman modulation contrast and fluorescence with ex/em 480/520 nm. The 324 images were compiled into a dataset referred to as a stack.

The acquired images were digitally enhanced using MetaMorph Image Analysis System (Universal Imaging, Westchester, PA). Each image contained 35 analyzable microwells corresponding to 35 regions created using MetaMorph to digitally surround each microwell of interest. For each stack, a standard cell projected surface area was determined by randomly choosing over 100 cells and averaging their respective areas, which were determined using MetaMorph. Then for each of the images of a particular stack the 35 regions were appropriately placed on the array, followed by the image thresholded for bright areas to segment the cells from the remainder of the image. The software was then used to determine the area of segmented cells within each of the 35 regions. An integrated morphometry analysis application within MetaMorph was able to properly distinguish the cells from the autofluorescing microarray walls, minor cell fragments, and imperfections in the images using preestablished elliptical and size factors. The raw data containing the standard area count and the image and region location were directly sent to an Excel (Microsoft, Seattle, WA) spreadsheet for further analysis. A C-language program was written to compile raw data into formatted data describing the number of cells per individual microwell for a particular image-stack. The compiled data for multiple stacks describing individual cell fates were then sorted accordingly and used to produce various descriptive plots. Image analysis system accuracy was determined by random selection and manual analysis of 20 fields for comparison to the corresponding data generated by the computer. Spatial mapping of the cell distribution within the chamber was performed with Matlab (MathWorks, Natick, MA).

Statistical Analysis

Error bars represent standard error of the mean. Plot generation and curve fitting were performed on SigmaPlot (SPSS, Chicago, IL). The correlation coefficient was determined from the covariance of two datasets divided by the product of their standard deviations, σ:

$$\rho_{x,y} = \frac{\frac{1}{n}\sum_{i=1}^{n}(x_i-\mu_x)(y_i-\mu_y)}{\sigma_x \sigma_y}$$

where μ is the mean of the variable.

Model of Oxygen Concentration in Rose Chamber

The oxygen transport from the atmosphere through the silicone gasket and into the media was modeled by dividing the problem into two parts, the rate of oxygen diffusion through the gasket and the diffusive transport of oxygen throughout the cell culture chamber. To determine the oxygen concentration on the inside surface of the gasket, we calculate the overall molar diffusive flux through the gasket with oxygen uptake by the plated cells. By assuming the overall molar flux through the gasket is equal to the oxygen consumption rate, we obtain:

$$N''_{O_2,r} = \frac{P_{O_2,rubber}}{R_{out} - R_{in}}\left(p_{O_2,R_{out}} - p_{O_2,R_{in}}\right) = \frac{Q}{A_{gasket}} \qquad (1)$$

where $N''_{O_2,r}$ is the molar flux of oxygen in the r direction, $P_{O_2,rubber}$ is the permeability of silicone rubber to oxygen, R_{out} and R_{in} are the outer and inner radius of the gasket respectively, $p_{O_2,R_{out}}$ and $p_{O_2,R_{in}}$ are the partial pressures of

oxygen at the outer and inner radius, Q is the oxygen uptake rate of the chamber, defined by $Q = V_{\max}\pi R_{in}^2\rho$, where ρ is the cell density and $V_{\max}$ is the maximal oxygen uptake rate per cell, and A_{gasket} is the surface area of the gasket–media interface. The use of the $V_{\max}$ in this model was an overestimate of total oxygen consumption, but allowed the calculation of the maximal possible oxygen gradient. A more thorough description would use Michaelis-Menten uptake kinetics. The partial pressure of oxygen at the boundary of the rubber–media interface can be related to the molar concentration of oxygen at the interface using Henry's Law:

$$c_{O_2,R_{in}} = \frac{p_{O_2,R_{in}}}{k_{O_2}}, \tag{2}$$

where $c_{O_2,R_{in}}$ is the oxygen concentration at the gasket wall and k_{O_2} is Henry's constant for oxygen in water at 37°C. The specific parameters used in this model are listed in Table I. The $c_{O_2,R_{in}}$ is used as a boundary condition in determining the oxygen distribution in the culture chamber. By assuming an axisymmetric, steady-state chamber, we can model the concentration of oxygen using a nondimensional binary diffusion equation in cylindrical coordinates:

$$\begin{gathered}\frac{\partial}{\partial\hat{r}}\left(\hat{r}\frac{\partial\hat{c}}{\partial\hat{r}}\right) + \frac{\partial^2\hat{c}}{\partial\hat{z}^2} = 0 \\ 0 \le \hat{r} \le 1 \\ 0 \le \hat{z} \le 1\end{gathered} \tag{3}$$

where $\hat{c}$ is the dimensionless concentration with respect to the concentration at the gasket-media interface, $c_{O_2,R_{in}}$, where $\hat{c} = (c - c_{O_2,R_{in}})/c_{O_2,R_{in}}$, and $\hat{r}$ and $\hat{z}$ are the dimensionless coordinates defined by $\hat{r} = r/R_{in}$ and $\hat{z} = z/H$ where R_{in} is the inner radius of the gasket and H is the chamber height. The boundary conditions are given by:

$$\frac{\partial\hat{c}}{\partial r}(0,\hat{z}) = 0, \qquad 0 \le \hat{z} \le 1, \tag{4}$$

$$\frac{\partial\hat{c}}{\partial\hat{z}}(\hat{r},0) = 0, \qquad 0 \le \hat{r} \le 1, \tag{5}$$

$$\frac{\partial\hat{c}}{\partial\hat{z}}(\hat{r},1) = Da, \qquad 0 \le \hat{r} \le 1, \tag{6}$$

$$\hat{c}(0,\hat{z}) = 0, \qquad 0 \le \hat{z} \le 1, \tag{7}$$

The boundary conditions describe a system with no flux at the top of the chamber, a constant oxygen concentration at the gasket wall, a constant oxygen flux at the cell surface, and no flux at the center of the chamber, which describes the axisymmetric condition. The Damkohler number (Da) is the nondimensional oxygen flux defined in this case as the ratio of the maximal oxygen uptake rate and the diffusion rate (Allen and Bhatia, 2003), given by:

$$Da = \frac{\rho V_{\max} H}{D c_i}, \tag{8}$$

Equations 3–7 are a homogenous differential equation with nonhomogenous boundary conditions that may be solved analytically. The solution is based on the general solution to Laplace's equation in cylindrical coordinate with a nonhomogenous boundary condition on the bottom (Haberman, 1998). The complete solution for the oxygen concentration profile is:

$$\hat{c}(\hat{r},\hat{z}) = 2Da\sum_{n=1}^{\infty}\frac{J_0(\hat{r}\sqrt{\lambda_n})}{\lambda_n J_1(\sqrt{\lambda_n})}\left(\frac{\cosh(\hat{z}\sqrt{\lambda_n})}{\sinh(\sqrt{\lambda_n})}\right) \tag{9}$$

where J_0 and J_1 are the Bessel functions of the first kind of order 0 and 1, respectively, and $\lambda_n = z_n^2$, where z_n here represents the nth zero of $J_0(z)$.

Model of Cytokine Diffusion within the Rose Chamber

The maximum effective signaling distance of the cytokine was defined as the distance from the signaling cell where the concentration became equal to the minimum concentration of the cytokine required for cell survival and proliferation. Assuming a solitary cell in a well, the effective signaling distance from the cell from Fick's diffusion equation was derived in a simplified model. The full derivation of the effective signaling distance is presented elsewhere (Francis and Palsson, 1997). Here, we have adapted their equation to calculate the effective signaling distance:

$$L_{crit} = \frac{F_{tot}}{D_{CCg}K_m} \tag{10}$$

where L_{crit} is the critical length for minimum effective signaling, F_{tot} is the molar secretion rate of cystatin C (CCg), a required secreted factor for AHP survival, per cell, and K_m is the minimum effective concentration of CCg. The diffusion constant for CCg was estimated from its molecular weight (Young et al., 1980), while other parameters for this model were derived from (Taupin et al., 2000). The secretion rate, F_{tot}, was unknown, but a possible range of rates were calculated by estimating the possible range of times required to achieve the minimum CCg concentration required for cell survival and proliferation from the minimum concentration of cells required for survival. The parameter F_{tot} assumed that all of the CCg secreted by the cell diffused out of the well rather than remaining within the well. Once an effective signaling distance was obtained, the time

Table I. Model parameters.

Modeling parameter	Value	Units	Source
D_w, O_2 diffusivity in water	2×10^{-5}	cm^2/s	(Allen and Bhatia 2003)
P_{O_2}, O_2 permeability in silicone rubber	4.38×10^{-6}	cm^3(STP)/cm^2/cm/s* bar[a]	(Brumels et al. 2003)
k_{O_2}, Henry's constant for oxygen in water at 37°C	5.25×10^4	bar	(Incropera and De Witt 2002)
V_{max}, max O2 uptake	3.06×10^{-17}	$molO_2$/s/cell	(Kallos and Behie 1999)
$P_{O_2,R_{out}}$, partial pressure of O2 in atmosphere	0.21	bar	
H, height of chamber	0.3	cm	
R_{out}, outer radius of rubber gasket	1.75	cm	
R_{in}, inner radius of rubber gasket	1.25	cm	
ρ, cell density on Day 0	3.43×10^3	cells/cm^2	
D_{CCg}, diffusivity of CCg in media	9.00×10^{-07}	cm^2/s	(Young et al. 1980)
K_m, minimum effective bulk cytokine concentration	0.2	ng/mL	(Taupin et al. 2000)
ρ_{min}, minimum cell concentration without conditioned media	1666.67	cells/mL	(Taupin et al. 2000)

[a]Where cm^3 (STP) is the amount of gas in 1 cm^3 at standard temperature and pressure (273 K, 1 atm).

associated with reaching this distance may be calculated using the equation for random Brownian motion:

$$t = \frac{L^2}{2D_{CCg}}, \tag{11}$$

where t is the time it takes for a signal to reach a certain distance L.

RESULTS

Design Criteria

Characterization of Microarray Platform

Our culture platform consisted of a microfabricated bottom coverslip, an oxygen-permeable gasket, an unpatterned top coverslip, and a top and bottom aluminum anchor plate (Fig. 1A,B). The microfabricated coverslip contained microwells that were the dimensions of the photolithography mask used to create the pattern. The pattern on the microfabricated coverslip could be altered with different mask configurations. The microwells created a nondegradable pattern that only permitted localized regions of cell contact. Upon application of fluid flow, cells at the bottom of a well were protected from convective removal, whereas cells that protruded from the walls were not. This type of patterning did not rely on integrin-mediated selective adhesion, in contrast to conventional micropatterning methods.

For this study, SU-8, a negative-tone epoxy resin photoresist, was employed to build our structures. Once fully cross-linked, SU-8 is a stable material that is very difficult to degrade or remove. The stability of the material suggested pattern degradation would be minimal. In addition, the thickness and patterns were easily tunable during the spinning and photolithography process. The thickness of our SU-8 layer was measured to be 50–100 μm, but can be spun to be as thick as 2 mm (Che-Hsin et al., 2002). Recent reports have suggested that the fully cross-linked material is noncytotoxic and relatively inert (Heuschkel et al., 1998; Voskerician et al., 2003; Wakamoto et al., 2001). Finally, SU-8 is transparent, with a refractive index of 1.67, permitting light microscopy on the entire surface of the substrate with minimal aberrations at a 50 μm thickness.

The array design chosen for this study had square wells with 90 μm sides, for a total available area of 8,100 μm^2. Alternative dimensions and shapes could be rapidly prototyped, but these well dimensions were chosen to be the minimum size required by the estimated final number of cells per well. This dimension would maximize the number of wells for analysis, while also allowing room for growth. AHP cell diameter was estimated to be 10–15 μm from random image sampling. From this measurement, the projected surface area of a neural progenitor cell was estimated to be a maximum of 176 μm^2; therefore, a maximum of 46 cells could fit within the well. During short-term experiments (~4 days), this area was intended to ensure that cells did not overgrow the wells and that there was sufficient space for cell processes to be sent out. For a single cell with a doubling time of 24 h, this surface area would have been adequate to contain all the progeny for 6 days. For wells containing multiple cells or cells that doubled at a faster rate, however, this space would have been not been sufficient for containment. Other microarray dimensions were constrained by the emulsion mask resolution. The center-to-center distance between wells was 120 μm, creating 30-μm wide walls. The 30-μm resolution was the smallest reliable resolution achievable with an emulsion mask. Smaller features could be obtained with a higher resolution printer or a chrome mask. The wall thickness was reduced to a minimum to prevent cells from settling on the tops of the walls and disrupting the pattern. The accuracy of the photolithographic process was verified by comparison under microscopy to the original mask dimensions. In general, film thickness was within 5 μ of the desired thickness, and patterning fidelity was within 3–5 μ of the original dimensions (data not shown). The height of the walls, which defined the depth of the wells, ranged from

50–100 μm. These depths prevented significant cell migration between wells over short culture times (~days) in a height-dependent fashion. The aspect ratio of the wells, at 9:5 (width:height) for 50-μm walls, permitted a large cross-sectional area for diffusive exchange of nutrients and waste. To support the culture of AHPs, the patterned substrates were coated with poly-L-ornithine and laminin prior to cell seeding. The sequential coating protocol created an evenly adsorbed protein layer on the substrate that was verified by immunostain (data not shown).

Cellular Arraying

AHPs were seeded into microfabricated chambers to characterize the arraying process. High-density arrays were generated within minutes and semiautomated scans were taken after 5 h to prevent detachment during the scanning process. For clonal assays, arraying efficiency was determined by the fraction of microwells containing only one cell. When a concentration of 35,000 cells/mL was used, ~27% of the analyzed wells contained a single cell after the arraying process, corresponding to 3,098 wells out of the 11,340 analyzed. Of the remaining wells, 99% had either no cells (7,027 wells, 62% of total wells), two cells (887 wells, 10.4% of total wells), or three cells (230 wells, 2% of wells) (Fig. 1C). The remaining 1% of the wells contained greater than three cells/well. When a concentration of 20,000 cells/mL was used, similar trends were obtained, but there were a greater number of empty wells. In contrast, higher cell seeding densities resulted in a larger number of wells containing two or five cells. Microarrays that had smaller well dimensions contained a

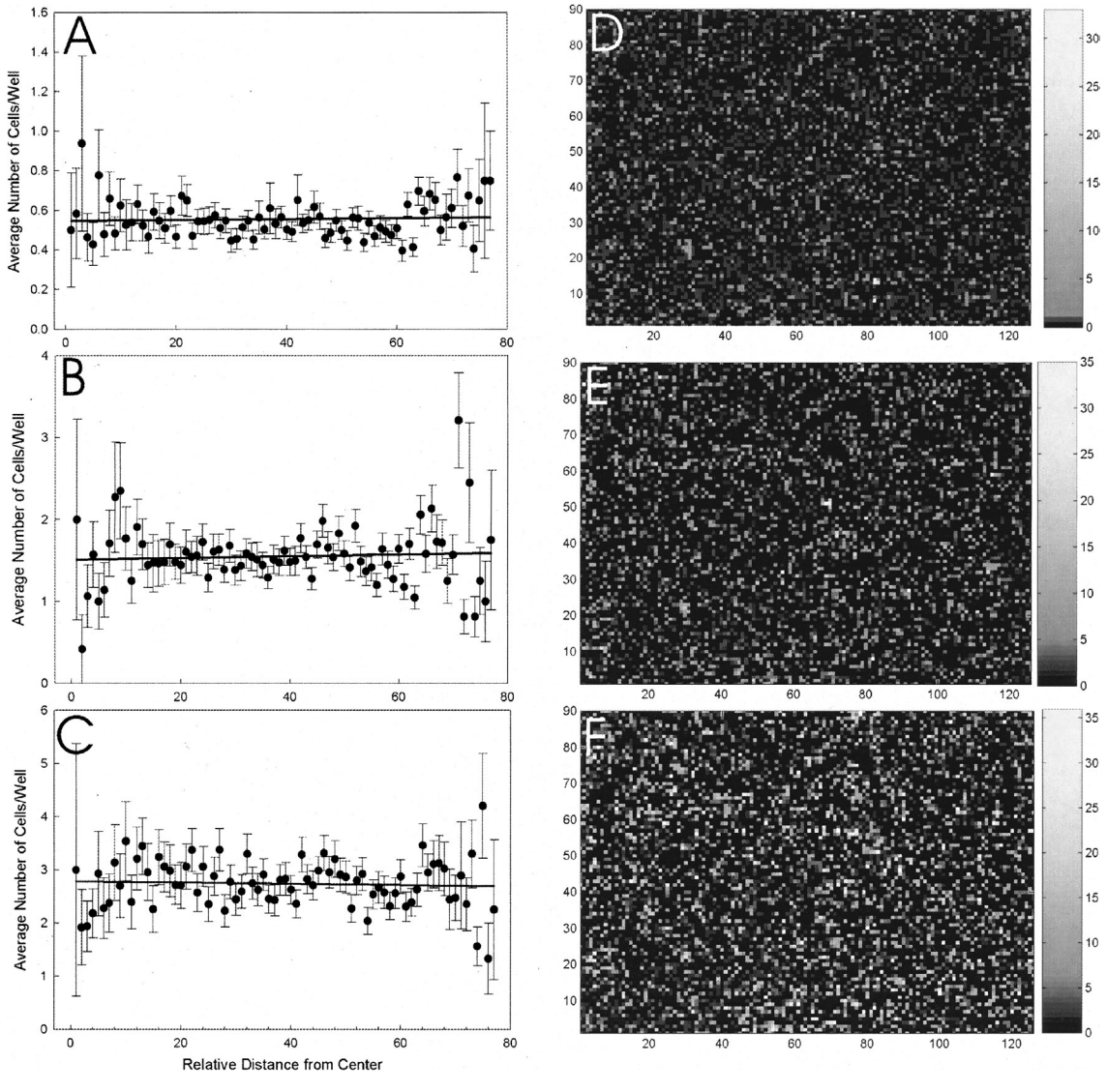

Figure 2. Spatial homogeneity in cell distribution. The average number of cells per well was tracked as a function of the relative distance from the center of the chamber on (**A**) Day 0, (**B**) Day 2, and (**C**) Day 4. The average number of cells increased over time, but the shape of the contour remained level, indicating relative spatial homogeneity. The cell population was mapped spatially with a grayscale indicating the number of cells per well in (**D**) Day 0, (**E**) Day 2, or (**F**) Day 4. Each square represents one well.

higher percentage of single cell wells due to the reduced surface area of each well (data not shown). After seeding the cells in the array, the cells were permitted to settle for 5 min. The calculated settling time for the cells in the chamber was determined from the equation for the sedimentation velocity of a sphere in an infinite fluid (Denn, 1980). From the maximum height of 3 mm (chamber height), the maximum time to settle was ~7–15 min, where the density of a cell was 1.06 g/mL and the cell diameter ranged from 10–15 μm. To reduce the number of multicell wells, the arraying time permitted most, but not all, cells to settle. Overall, our data indicated that the three major factors controlling arraying efficiency and number of cells per well were pattern dimensions, sedimentation time, and cell seeding concentration.

To verify that the inhomogeneous laminar flow profile during cell seeding did not generate an inhomogeneous cell distribution, the variations in cell number and growth as a function of location were determined. The average number of cells per well as a function of distance from the center was determined for each day, and the regression lines through these data points have slopes ranging from −0.001 to 0.001, which indicated a constant cell number per well regardless of distance (Fig. 2A–C). The average cell number per well was 0.54 cells/well for Day 0, 1.5 cells/well for Day 2, and 2.8 cells/well for Day 4. The cell number per well was measured and plotted in a location map such that the distribution of cells across the chamber could be seen graphically. From the measured wells, the distribution remained random over time (Fig. 2D–F).

Another measure of arraying efficiency was the fraction of cells seeded that remained adherent after 5 h. We estimated ~17,000 cells were arrayed over 4.9 cm^2, or 32% of the ~52,500 cells in the seeding media. This adherent density exceeds the minimum density requirements for survival in conventional neural progenitor cell culture in FGF-2 by ~7-fold. Thus, the platform required higher cell seeding density than conventional cultures, but enabled single cell survival and tracking due to a high "effective" cell concentration in the chamber.

Oxygen and Cytokine Concentration Models

To ensure proper growth of neural progenitor cells within the chamber, the oxygen and CCg concentrations within the chamber must remain at sufficient levels. For oxygen, as dissolved oxygen within the media is consumed the cells are dependent on oxygen diffusion through the silicone gasket for survival. Rubber, particularly silicone rubber, is highly permeable to oxygen. The permeability of oxygen in silicone is roughly equal to the solubility and diffusivity of oxygen in water (Krevelen, 1990). For standard oxygen uptake rates of neural progenitor cells (Kallos and Behie, 1999), the 3-mm thick silicone gaskets used permitted sufficient oxygen transport for AHP survival at a cell density of 10^3–10^4 cells/cm^2 and an ambient oxygen concentration of 160 mmHg. The partial pressure of oxygen at the gasket–media interface is not significantly less than the atmospheric partial pressure of oxygen. Equation 9 is numerically solved and plotted in Figure 3A. At the cell surface boundary, the oxygen concentration steadily decreases to a minimum at the center of the chamber. However, at the Damkohler numbers calculated, the minimum oxygen concentration in the chamber was calculated to be more than 99% of the initial interface concentration. As the ratio between the oxygen uptake rate and the diffusion rate, a low Damkohler number indicates that oxygen transport to the cells is not diffusion limited. At steady state, the oxygen partial pressure within the chamber is near atmospheric (158–160 mmHg), and all cells should have sufficient oxygen levels for survival and growth. This model, combined with the experimentally determined homogeneity of growth across the chamber, suggests that there were no significant oxygen gradients in the chamber.

In contrast, the cytokine concentration in the chamber was dependent on the cytokine secretion rate of each cell. Cells in the microfabricated culture system shared a common pool of bulk media. By drawing from paracrine signaling factors from neighboring cells and the bulk media, much like in a standard culture plate, low numbers of cells in each microwell were able to survive and proliferate, as opposed to other high-throughput plate assays that do not allow for soluble factor exchange. The chamber was completely filled with media, thus reducing the convective transport of secreted factors due to motion in the media.

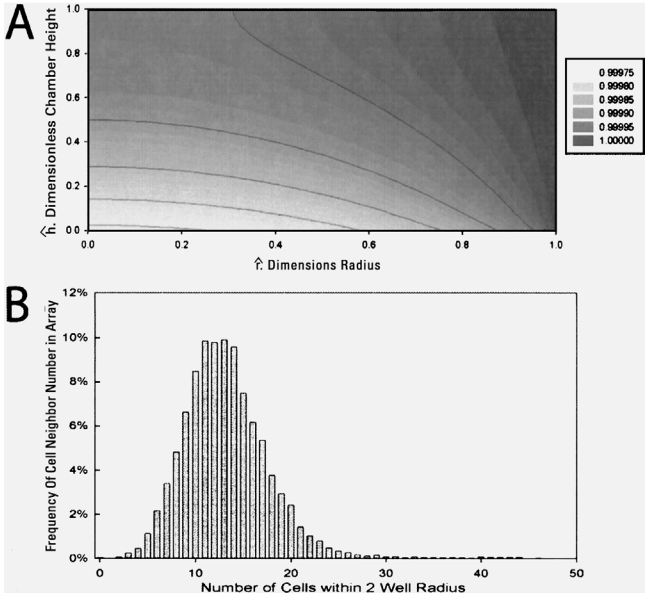

Figure 3. Oxygen and cytokine gradients. **A:** 2D contour plot of the predicted dimensional oxygen concentration at a radial cross section of the chamber. In the graph, the y-axis, the cell layer is at $\hat{h} = 0$, in contrast to the model definition. The output shows the $-\hat{c}$ where $c_{O_2,R_{in}}$ is 1.32×10^{-3} mol/L. **B:** In order to assess the potential for paracrine signaling, we quantified the relative position of cells within the chamber (see text for details). The frequency of the total number of cells within a two-well radius of each monitored well in the chamber on Day 0. 92% of the counted wells had between 6 and 19 cells in the radius.

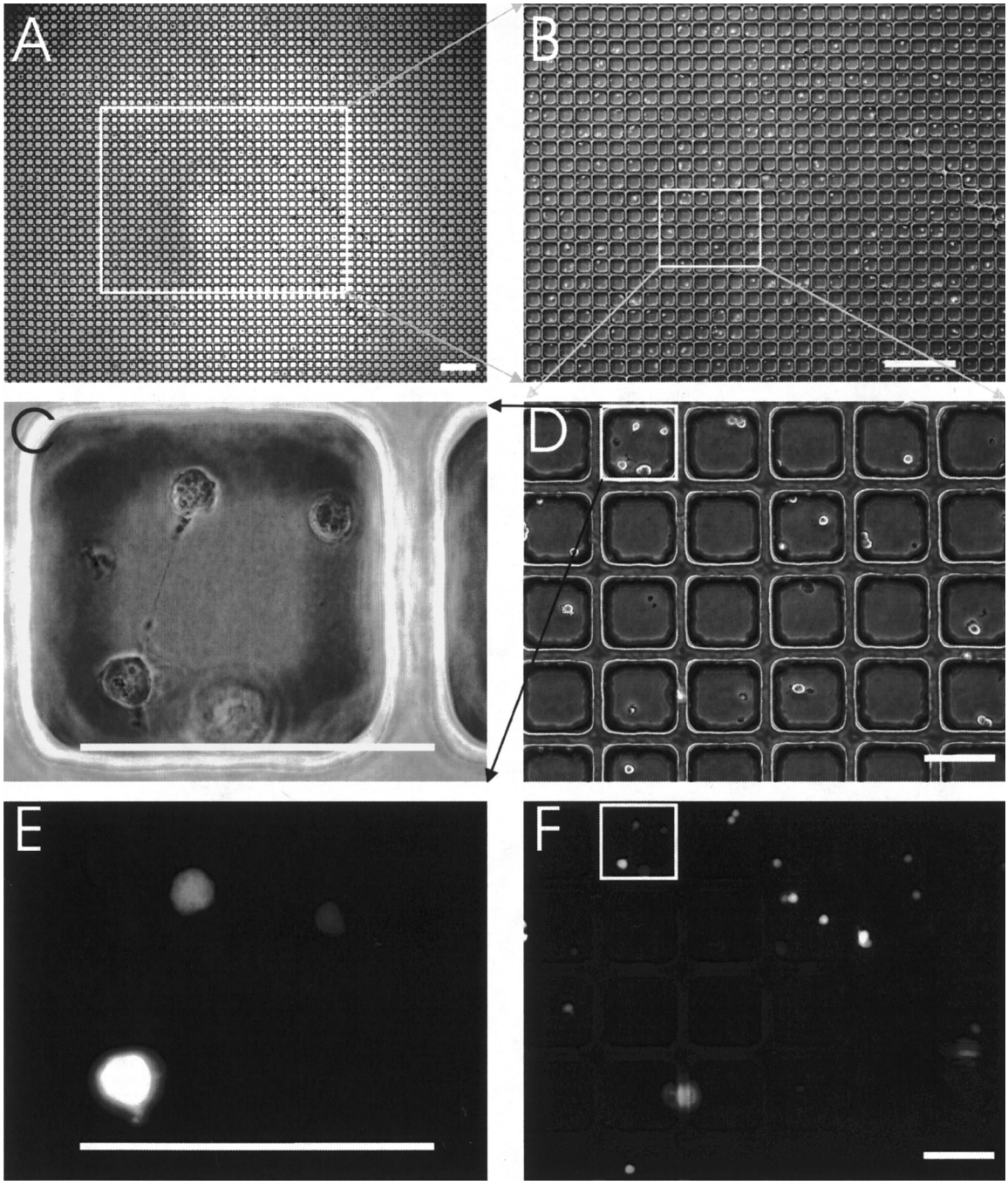

Figure 4. Different magnifications of the same field of AHPs. **A:** A low-magnification image of microfabricated array to illustrate the scale of the system. Scale bar = 500 μm. **B:** A higher magnification image of **A** where distinct cells can be seen. Scale bar = 500 μm. Areas of interest can be marked and studied at higher magnifications. **C:** A high numerical aperture image of a single well, outlined in white in **D**. This image was taken with an oil immersion 100× objective to demonstrate the compatibility of the system with high numerical aperture (NA) objectives. **D:** A higher-magnification image of the area outlined in white in **B**. Cellular interactions can be studied at this magnification (20× objective). **E:** Fluorescent image of the same field in **C** to show detection of GFP+ AHPs. **F:** Fluorescent image of the same field in **D**. Scale bars in **C**–F = 100 μm.

Some convective transport was introduced during the image acquisition every 48 h through movement to and from the microscope, the motorized stage movements on the microscope, and variations in temperature outside the incubator. However, during the majority of the experiment the transport of soluble factors in the chamber was dominated by diffusive transport. To determine the extent to which local signaling gradients affected the microenvironment within the chamber, the effective diffusion distance and its associated diffusion time for CCg, a secreted cytokine required for survival, were estimated. The effective diffusion distance was defined as the distance from the secreting cell at which the secreted cytokine concentration fell below the minimum effective threshold. The

signaling distance was directly proportional to the cytokine secretion rate, for which a range was estimated. This range was based on the assumption that the minimum cell density could secrete the minimum concentration of CCg within 2–12 h. This time range was selected assuming that paracrine signaling was required for survival within hours of seeding. The calculation of these parameters indicated an effective signaling range of 900–80 μm and times of 1.5 h to 30 sec, respectively, to reach the minimum signaling concentration, K_m, at these diffusion distances. From this analysis, one cell appeared to generate a cytokine gradient that possibly extended from a minimum of one well to a maximum of seven wells away from the secretion point. Based on the mapping of the cells in wells on Day 0, 92% of the wells had 6–19 cells within a two-well radius (Fig. 3B). Paracrine secretion from multiple cells at this distance would be sufficient for survival and proliferation. Although each individual cell has a cytokine concentration gradient, the homogenous spacing of the cells across the chamber results in minor, local variations of cytokine that are periodically disrupted due to chamber handling. Convective transport through chamber handling and temperature transitions between 37°C and 20°C (room temperature) mixed the cytokines within the chamber, creating a more homogenous cytokine microenvironment. However, within seconds to 1–2 h of the end of convective transport effects, diffusive gradients were reestablished within the chamber. Thus, cytokine transport within the chamber was through

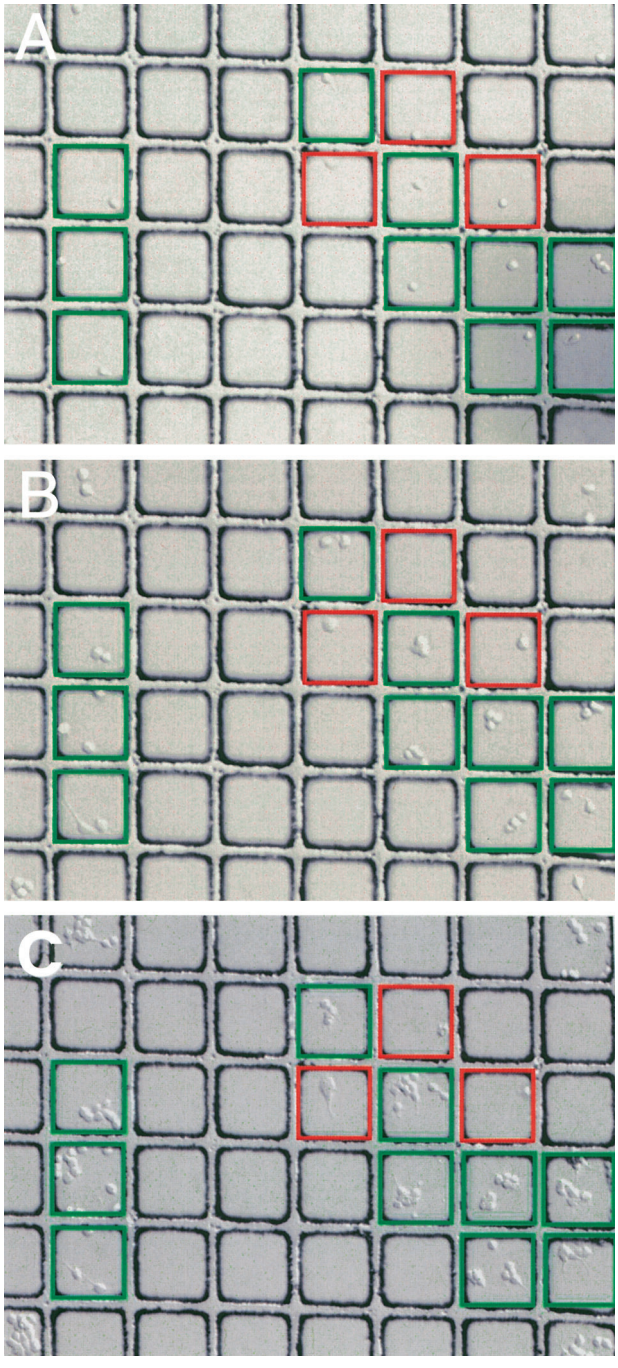

Figure 5. Tracking AHPs in the microarray. Cells were tracked over 6 days using the automated microscopy system. A sample frame of the culture is shown on (**A**) Day 0, (**B**) Day 2, and (**C**) Day 4. Green boxes indicate wells that contain proliferating cells. Red boxes indicate wells that contain nonproliferative cells.

Table II. Comparison of computer and manual cell counting.

A

	Correlation coefficient
Day 0	0.91
Day 2	0.88
Day 4	0.89
Day 6	0.89

B

Manual cell count	Computer averaged count	±SEM
0	0.24	±0.02
1	1.47	±0.07
2	2.43	±0.08
3	3.52	±0.17
4	4.44	±0.23
5	5.57	±0.32
6	6.44	±0.30
7	6.91	±0.35
8	9.36	±0.56
9	9.38	±0.54
11	11.35	±1.04
12	10.60	±1.13
13	13.40	±0.99
14	15.22	±0.81
15	13.67	±1.48
16	19.00	±2.63
17	17.75	±2.02
18	18.00	±3.30
19	16.67	±2.03
20	21.00	±2.74
21	18.83	±1.89
22	26.57	±2.74
23	26.00	±3.87
24	25.00	±3.08
25	24.50	±3.18
26	23.67	±2.19

a combination of diffusive and convective transport, with diffusive transport dominating during the majority of the experiment.

Neural Progenitor Growth in the Platform

Neural Progenitor Cell Culture in Microfabricated Chamber

AHPs were cultured in the microfabricated chamber in media containing FGF-2 for a minimum of 4 days. During this time, the programmable microscope system scanned the stage and acquired images of the arrayed cells every 48 h. In addition to the semiautomated scanning microscope system, higher-magnification images could be obtained of cells of interest. The Rose chamber permitted high-magnification observation of cells in culture while maintaining sterility. In this manner, cell morphology and GFP expression and distribution could be examined in detail (Fig. 4E,F). In contrast, low-magnification images permitted rapid evaluation of a large portion of the array to determine regions or wells of interest (Fig. 4A–D). Figure 5A–C is typical of the overwhelming majority of the images taken. Obtained through the scanning microscopy method, the automated stage was able to reproducibly scan the array at each time point. We were able to obtain a clear, consistent image in phase contrast and fluorescence (data not shown) that could undergo further image analysis. The time course over 4 days in Figure 5A–C also showed normal, proliferating AHPs on the microfabricated array, demonstrating the compatibility of the system to neural progenitor and stem cell growth. Observation of the culture over this time also demonstrated the autonomy and physical isolation of the majority of the cells in the wells during the experiment.

In the 50-μm deep wells, ~10% of the wells contained cells that migrated from their original well at each time point under the conditions utilized in this study. Rat neural progenitor cells are adhesion-dependent and migrate at finite rates in monolayer plate culture. Without limiting walls, a single cell can give rise to a colony that is spread

Table III. Cell counts per well for field shown in Figure 3 where A–E indicates row position, and 1–7 indicates column position beginning in the upper left hand corner.

Well	Day 0	Day 2	Day 4
A1	1	3	3
A2	0	0	0
A3	0	0	0
A4	0	0	0
A5	0	0	0
A6	0	0	0
A7	1	2	10
B1	0	0	0
B2	0	0	0
B3	0	0	1
B4	1	3	2
B5	1	0	0
B6	0	0	0
B7	0	0	0
C1	1	2	4
C2	0	0	0
C3	0	0	0
C4	1	1	0
C5	2	2	9
C6	1	1	1
C7	0	0	0
D1	0	3	2
D2	0	0	0
D3	0	0	0
D4	0	0	0
D5	1	2	3
D6	0	0	0
D7	3	2	4
E1	1	2	2
E2	0	0	0
E3	0	0	0
E4	0	0	0
E5	0	0	0
E6	1	1	5
E7	2	2	6

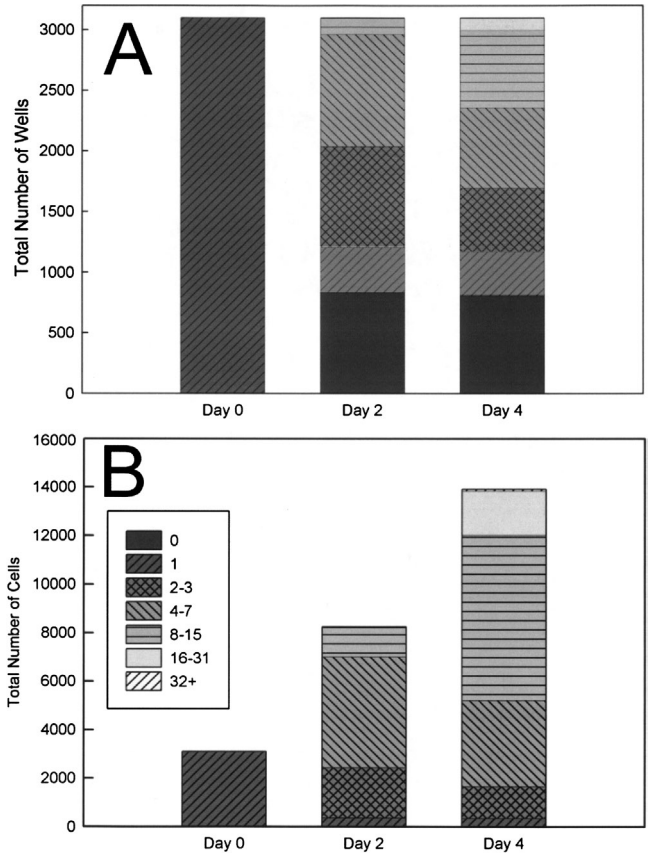

Figure 6. Analysis of single-cell populations. Single cell wells were identified on day 0 and analyzed over 4 days in culture. The cell populations have been segmented into categories based on the number of progeny. **A:** The population distribution (number of wells) derived from single-cell clones over time. **B:** The population distribution (total number of cells) derived from single cell clones over time.

over 500 μm after 5 days (Palmer et al., 1999). We reduced the cell migration to 3% of the wells per day by increasing the well height to 100 μm from 5 μm. In addition, cell migration decreased to 3% of the 50 μm height wells per day after the seeding density was reduced to 17,500 cells/mL.

Automated Image Analysis of the Microfabricated Array

In initial experiments, cell fate analysis was performed manually in a comparable manner to 96-well plate assays. However, manual tracking of 12,000+ wells was prohibitively time-consuming and susceptible to user bias. We therefore adapted a commercial package (MetaMorph Imaging System) to create a semiautomated cell tracking system. For each stack of images at each timepoint, a standard cell projected surface area was determined by averaging over 100 randomly chosen cells. To determine the number of cells per well, the GFP+ segmented area in each well was divided by the average cell area. The accuracy of the computer analysis was determined by comparison to manual counts over 20 random fields (corresponding to 700 wells) per stack. The correlation coefficient of the system for day 0, day 2, and day 4 was calculated to be 0.90, 0.88, and 0.89, respectively (Table IIA). This indicated a good agreement between the manual count and the computer analysis. Accuracy per cell number demonstrated the absolute decrease in accuracy as the number of cells per well increases (Table IIB). However, the error remained proportional to the cell number. Once in spreadsheet format, wells may be individually tracked. Table III shows the image analysis output for the field shown in Figure 5A–C. Further analysis of the extracted data was conducted to study population dynamics and explore specific hypotheses.

Single Neural Progenitor Cell Proliferation

To demonstrate the degree of proliferation heterogeneity in the AHP population, we analyzed the contents of wells containing a single cell on Day 0. Proliferative heterogeneity has been demonstrated before in GFP+ neural progenitor cells using a smaller sample size (Palmer et al., 1999). The data were segmented according to the number of daughter cells found on a given day (i.e., 0–2, 2–4, etc.). Therefore, wells in which there was cell death contained

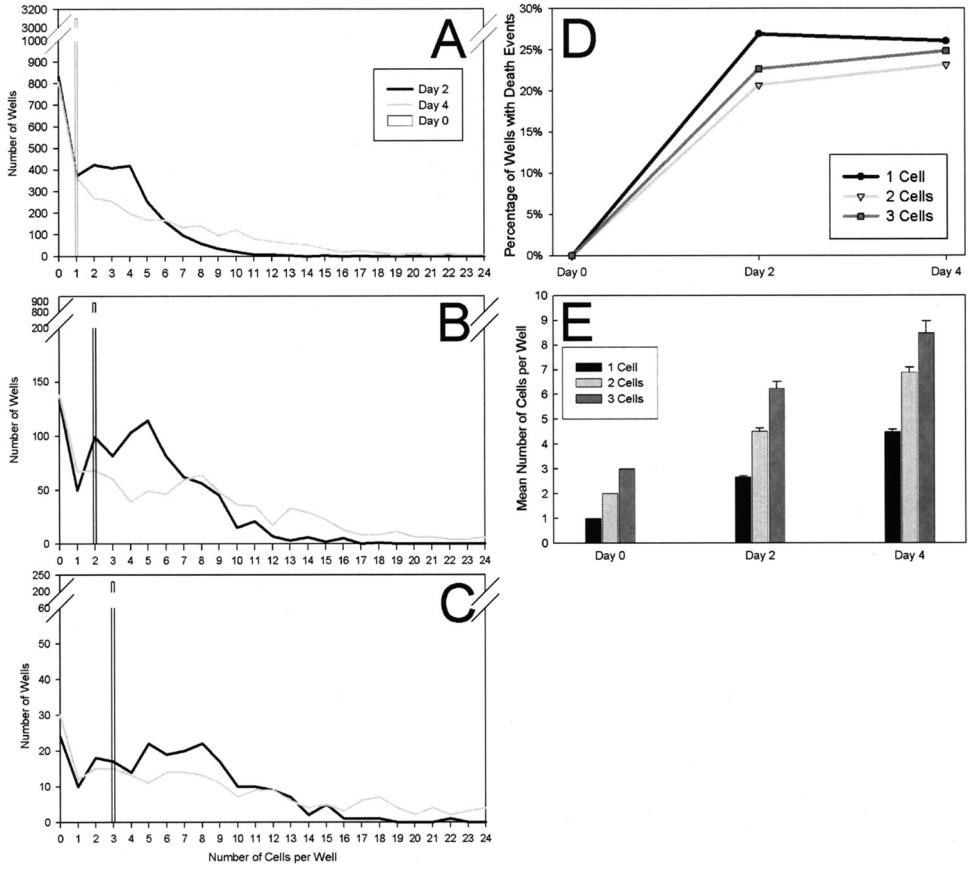

Figure 7. Population distribution over time of different starting populations. Wells were segmented by number of cells per well (1, 2, or 3) on Day 0. The distribution of cell number per well is shown for each time point (Days 0, 2, 4). **A:** One-cell wells. **B:** Two-cell wells. **C:** Three-cell wells. **D:** The percentage of analyzed wells with a "death event" where "death event" frequency was calculated based on the number of wells with less than its starting cell number. **E:** Mean cell number ± SEM of segmented populations (starting 1, 2, or 3 cells per well) over time.

0 cells in subsequent days, whereas cells that underwent three cycles of cell division contained ~8 cells. In the following results, it is important to note that neural progenitors are relatively motile cells and a small (10%), but significant, fraction of the cells migrated from their well per day. Due to this migration, the clonal status of any particular well cannot be verified. Thus, the trends in the data presented reflect a population of cells where the lineage of a majority, but not of all, of the cells could be tracked.

Figure 6A shows the total number of wells that began with one cell and the distribution of the segmented cell populations evolving over time. We scored wells that contained one cell on Day 0 and zero cells subsequently as "cell death" events. After the start of the experiment, "cell death" occurred in 27% of the wells, but no further significant cell death occurred after Day 2. By Day 2, a small fraction of wells (4%) contained 8–15 cells, indicating at least three population doublings. Similarly, by Day 4 a small fraction of wells (3%) contained 16–32 cells, indicating 4–5 population doublings. These data suggest a wide range of responses (survival, proliferation rate), with a subset of cells in this AHP population dividing approximately every 12 h.

These data could be further examined from a population perspective. Figure 6B tracks the growth of cells that began as clonal cultures. The overall cell population increases linearly, rather than exponentially, over the course of the experiment, due to the overlapping processes of cell death, quiescence, and proliferation in the culture. Furthermore, it is apparent that rapidly proliferating subpopulations constitute an increasing proportion of the population with time. For example, by Day 4, 62% of the population was derived from just 23% of the initial population, demonstrating the importance of the rate of proliferation in determining the final composition of the culture (or tissue, in vivo) (Jacquez, 1972).

Neural Progenitor Cell Proliferation Tracking

To explore the hypothesis that local cell–cell interactions may play an important role in survival, proliferation, or differentiation, we compared wells containing single cell clones to wells containing 2 or 3 cells on Day 0 (Bhatia et al., 1999; Nelson and Chen, 2002; Tsai and McKay, 2000). It is important to emphasize that this analysis required no additional experimentation; rather, the results seen in Figure 7 arose from a simple segmentation of data obtained during semiautomated analysis (Fig. 6).

Population histograms were obtained by scoring the number of wells with a given number of progeny (e.g., 1,2,. . .24) on Days 0, 2, and 4. Histograms were generated for wells that contained one, two, and three cells on Day 0. Figure 7 indicates similar trends for all three conditions. For single cell wells (Fig. 7A), the majority of wells contained 1–5 cells on Day 2. On Day 4, the distribution flattened as these cells underwent proliferation and varying degrees of cell death. Similar results were observed for two-cell wells, with a shift of the population peak to larger cell numbers as expected (Fig. 7B). On Day 2, a peak centered around 2–8 cells per well. For three-cell wells, a more diffuse peak centered around 5–9 cells per well was present at Day 2. By Day 4, wells that initially contained three cells had a wide distribution of constituents (Fig. 7C). Collectively, these data form a quantitative description of

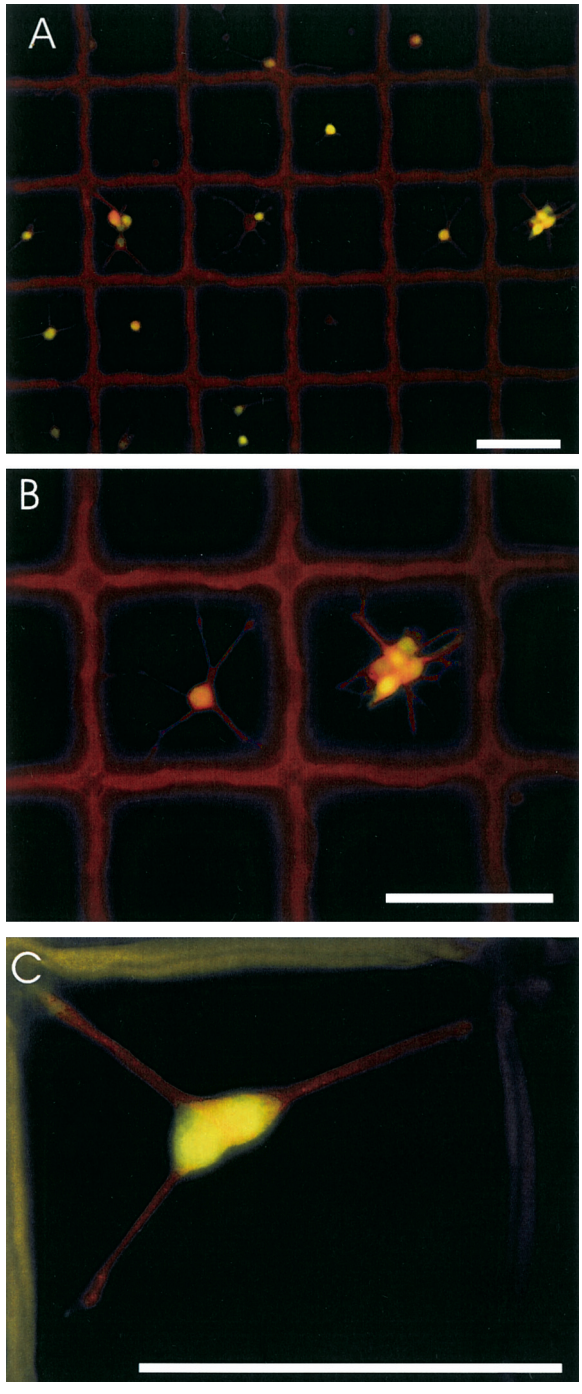

Figure 8. Differentiation of adult AHPs in the microfabricated array. GFP+ cells were differentiated along the neuronal lineage and stained for early neuronal marker Tuj1 (red) and astrocyte marker GFAP (blue). Few GFAP positive cells were seen in this preparation. Scale bar = 100 μm in **A–C**.

the survival and proliferation kinetics of AHPs both alone and with neighboring AHPs under defined conditions. These data can be used to examine hypotheses on the role of specific mitogens or soluble factors in modifying survival, cell–cell interaction, and proliferation.

As a specific example, we investigated the hypotheses that initial cell–cell interaction confers either 1) a survival advantage to AHPs, or 2) an increase in proliferation rate. We quantified survival indirectly by tracking net cell death. In these experiments, we recorded a "death event" if a well contained fewer cells than it did at Day 0. Thus, for three-cell wells, the wells that contained one or two cells at a later time point were scored as wells with death events. Death events were also scored when a cell had a markedly diminished diameter and no longer met our criteria for average cell size, or became nonfluorescent from lack of GFP production. The occurrence of a death or apoptotic event was measured across all wells (Fig. 7D). Using these criteria, there was no significant difference in the survival of one-, two-, and three-cell wells on Days 2 and 4. All three of the cell populations also grew at linear rates (Fig. 7E); however, population doubling analysis revealed that two- and three-cell wells doubled significantly slower than cells in single wells. For example, single cell wells contained an average of four cells (2 PD) on day 4, whereas triplet cell wells contained an average of only eight cells (rather than 12 cells). Taken together, these findings seem to indicate that in this culture configuration, *local* cell–cell interactions confer no advantage in the survival or proliferation of these AHPs beyond the soluble paracrine factors available to all cells in the chamber.

Differentiation of Arrayed Neural Progenitor Cells

After 4 days of culture in media with FGF-2, selected cell cultures were switched to neuronal differentiation conditions (retinoic acid + forskolin) to demonstrate the ability to track differentiation within the array system. Figure 8 shows Tuj1+/GFP+ cells within the array at two different magnifications (where Tuj1 is an early neuronal marker), indicating the ability to perform high-magnification immunofluorescence on the microfabricated substrate, thereby enabling a totally integrated proliferation and differentiation analysis system.

DISCUSSION

Our aim was to create a cell culture platform that would enable the quantitative, parallel study of individual progenitor cell fates over time. To that end, a microfabricated cell-based assay platform was designed, constructed, and characterized for its utility in tracking adult hippocampal progenitor cell survival and proliferation. The microfabricated array was built with a transparent photoresist whose dimensions were easily tuned to modify the frequency of single cell wells and maximal colony size. The chamber was able to support the deposition, paracrine-dependent survival, proliferation, and differentiation of over 3,000 single cell clones. The culture chamber was fabricated with alignment markers and integrated with an off-the-shelf semiautomated microscopy system enabling rapid image acquisition and analysis with 90% accuracy and 10-fold less time than manual analysis. Models of the microenvironmental variables in the chamber indicated a relatively homogenous oxygen environment and, for each cell, local cytokine gradients that may span a few well diameters when convective transport is absent. Using this platform, individual wells were tracked over several days to produce a quantitative description of the population dynamics over time. Examination of the proliferative heterogeneity between clonal neural progenitor cell cultures revealed that a small (3–4%), highly proliferative fraction of cells might exist. Further analysis of different starting populations (one, two, or three cells) showed that overall population growth was not enhanced by proximity to other cells in this culture configuration. Finally, AHPs were differentiated within the chamber and imaged at high magnification through the coverslip bottom, enabling a continuous analysis system that could prove useful in the study of stem cells of various origins.

Microfabricated Platform Design and Implementation

We fabricated addressable SU-8 microwells on microscope coverslips that were integrated into a fluidic chamber and formed the basis of the 3D array platform. Our goal was to adapt 2D micropatterning techniques to confine a proliferative, motile cell population over many days. Furthermore, for studies of progenitor cell heterogeneity, we sought to avoid the selection of cellular subpopulations inherent in micropatterning techniques that rely on selective adhesion of cells to protein-coated substrates. Other nonadhesion-dependent patterning methods, such as electrophoresis (Ozkan et al., 2003), dielectrophoresis (Voldman et al., 2002), and optical methods (Flynn et al., 2002; Ozkan et al., 2003) have achieved rapid patterning ($\sim$ minutes), but the uncharacterized effects of active electric fields on some cells make this approach less attractive for some applications. Finally, SU-8 on glass offers an attractive alternative to opaque substrates (Powers et al., 2002) or optical fibers (Biran and Walt, 2002) due to its compatibility with traditional inverted microscopy. In conjunction with the image acquisition system, the semiautomated image analysis system increased the efficiency and effectiveness of the data analysis, allowing for larger sample sizes (11,340 wells analyzed per day) and removal of human bias. Conversely, semiautomation introduced $\sim$10% error due to flaws in the microwell fabrication. We expect that improvements in the microfabrication process (e.g., chrome mask) would reduce the error in subsequent designs. The adaptation of the platform to other experimental systems is straightforward, but several design tradeoffs must be considered. For example, cell density within the microfabricated array chamber is dependent on several factors. The cell concentration in the seeding medium dictates the number

of cells available for arraying. By increasing the cell concentration and the sedimentation time, the final cell density also increases. In the experiments described above, 32% of the cells seeded remained in the chamber. If cells were in limited supply, the fraction of cells remaining in the chamber could be increased by increasing the sedimentation time or agitating the seeding media to reposition unarrayed cells over a well. In addition, the wash media that contained unarrayed cells could be reapplied in a second arraying step. Conversely, increases in wash rate and well dimensions lead to changes in the flow profile that reduce the final cell density.

Variations in the microenvironment, such as oxygen and cytokine gradients, may influence the results of studies performed using 90-μm-square wells. Models were used to understand the degree of microenvironmental variation within the system. We have shown through a diffusion-reaction model that oxygen gradients within our system were predicted to be negligible. These predictions were supported by the observation that cell proliferation in the center of the chamber, where one would expect oxygen limitations to be most apparent, was equivalent to the rest of the chamber (Fig. 2). However, if a higher seeding density or a different cell type with a higher oxygen uptake rate were used, the oxygen gradient generated could cause hypoxia in the center of the chamber. Cytokine diffusion modeling of the secreted paracrine signals indicated the effective signaling distance of each cell was 80–900 μm, depending on the secretion rate. This model indicated the minimum spacing between cells for effective cytokine signaling via diffusion. Experimentally, within a two-well radius (240 μm) of each secreting cell, there were enough neighboring cells (6–19 cells) to provide enough CCg to promote survival at the beginning of the experiment. In adapting this platform to study secreted factor signaling in other cell types, the final cell density should be tailored to ensure adequate signaling between cells.

Notably, under the condition used in these experiments (well depth of 50 μm), 10% of the wells contained cells that migrated from their original well per day. Thus, the fate of any specific well could not be conclusively tracked. In this experiment, cell migration may be caused by cells overgrowing the microwells over time, or by dead cells that have detached and resettled in another well. We have been able to reduce cell migration through increasing the well height and reducing the seeding density, although a small percentage (3%) of cells still migrated in each reduction condition. Of possible concern, reduction of cells in the chamber would also reduce the number of cells analyzed. Other strategies to further reduce cell migration include shorter-term experiments that would permit cells less time to migrate or patterning the tops of the well walls with a molecule that inhibits cell migration, such as polyethylene glycol, agarose, or acrylamide (Chen et al., 1998). Thus, applications that benefit from quantitative, parallel analysis of many single cell clones, but can tolerate finite rates of cell migration, are well suited to this platform. In such cases, a miniaturized semiautomated array has clear advantages over conventional culture methods.

Neural Progenitor Cell Culture in Microfabricated Arrays

To demonstrate the ability of the microfabricated array system to maintain and track stem cell fates, we seeded, cultured, and tracked AHPs growth over 4 days. After 4 days, some chambers were cultured under neural differentiation conditions for an additional 4 days. The AHPs exhibited normal morphology and growth patterns in the microfabricated array culture chamber in comparison to previously published results of AHPs in traditional cultures (Gage et al., 1995a; Ray et al., 1993; Taupin et al., 2000) and were able to display early neuronal markers. Initial analysis of single AHPs cultured in FGF-2 at sufficient cell density for survival indicates that there is a large variation in the proliferative capacity of the cells, demonstrating the proliferative heterogeneity within neural progenitor cell culture. Heterogeneity within the neural progenitor cell population is well established (Chu and Gage, 2001; Suslov et al., 2002; Yaworsky and Kappen, 1999), but the source of this variation is unknown. Proliferative variation has been observed before with a small sample of cells (Palmer et al., 1999), and our data appears to confirm that a relatively small number of rapidly proliferating cells ($\sim$20%) can contribute disproportionately to the progenitor cell population (>60%), thus reinforcing the concept that continuous in vitro cultures of progenitor cell cultures may serve to select for a highly proliferative subpopulation. This study used proliferative dynamics as an indirect marker of subpopulations within a heterogeneous culture. This concept is supported by the longer doubling times of multipotent progenitor cells as compared to more rapidly dividing, yet more committed transiently amplifying progenitor cells (Morrison et al., 1997). Whether differences in proliferation rates correlate with other differences in these subpopulations (i.e., differentiation potential) remains to be determined; however, this platform may provide a useful tool for researchers searching for distinguishing characteristics of a heterogeneous population. The addition of known or putative mitogenic factors to this system may shift the proliferation profile and allow further functional segmentation of subpopulations.

We further applied this system to investigate the role of cell–cell interactions on AHP survival, proliferation, or differentiation by including two- and three-cell cultures in the data reanalysis. Cell–cell interactions are known to coordinate proliferation, differentiation, and apoptosis of neural stem cells in vivo, but their effect on cells in vitro has not been well studied (Doetsch, 2003; Hugnot et al., 2001). Although the multiple cell wells were not homogeneous, clonal populations, we completed this analysis as a proof-of-principle for investigating cell–cell interactions in a proliferative environment. Comparison of the single cell cultures to multiple cell cultures did not show an increase in proliferation rate due to cell–cell contact. Rather,

multiple cells proliferated more slowly on average than single cells. One possible hypothesis is that cell–cell contact may have inhibited progenitor cell growth in this culture configuration, due to the high overall cell density in the chamber (Freshney, 2000). However, a small percentage of two-cell wells proliferated rapidly, achieving four or more population doublings by Day 4 (Fig. 5B). Thus, the interplay between cell–cell contact and proliferative behavior in progenitor cells may be more complex than contact inhibition alone. Finally, we demonstrated the ability to perform immunofluorescent differentiation assays within the array format (Fig. 6). The capability to differentiate cells within the array enables the system to provide complete large-scale cell fate tracking from proliferation to differentiation.

SUMMARY

In summary, we have developed a microfabricated platform that enables parallel, quantitative analysis of stem cell proliferation and differentiation. This approach offers the ability to observe large numbers of single-cell cultures of adhesion-dependent stem cells that may not survive without paracrine signaling support. In addition, unlike multiwell plate platforms, large numbers of live cells may be observed using conventional microscopy and correlated with differentiated progeny by high magnification immunofluorescence in a rapid and efficient manner. We were able to track the proliferation of >3,000 single-cell cultures as well as survival and proliferation of progenitor cells as a function of initial cell population in a single experiment. Adaptation of this system to alternative cell types requires consideration of design criteria such as micropattern configuration, cell seeding concentrations, oxygen and cytokine gradients, and cell migration rates. Additional capabilities may be realized by incorporating existing technologies such as real-time gene expression through use of genetically encoded reporters (Torrance et al., 2001), integration with microfluidics to alter the fluidic milieu (Li Jeon et al., 2002), or incorporation of optical tools to interrogate cells of interest (Ozkan et al., 2003). Moving forward, robust interactions between technologists and stem cell biologists will be critical to the emergence and dissemination of enabling microscale tools.

We thank Vi Chu and Dirk Albrecht for helpful suggestions, Elliot Botvinick and Jagesh Shah for help with the Rose Chamber, and Christina Newcomb for help with the cell migration studies.

References

Allen JW, Bhatia SN. 2003. Formation of steady-state oxygen gradients in vitro: application to liver zonation. Biotechnol Bioeng 82:253–262.

Bajaj S, Welsh JB, Leif RC, Price JH. 2000. Ultra-rare-event detection performance of a custom scanning cytometer on a model preparation of fetal nRBCs. Cytometry 39:285–294.

Bhatia SN, Balis UJ, Yarmush ML, Toner M. 1999. Effect of cell-cell interactions in preservation of cellular phenotype: cocultivation of hepatocytes and nonparenchymal cells. FASEB J 13:1883–1900.

Biran I, Walt DR. 2002. Optical imaging fiber-based single live cell arrays: a high-density cell assay platform. Anal Chem 74:3046–3054.

Blake RA. 2001. Cellular screening assays using fluorescence microscopy. Curr Opin Pharmacol 1:533–539.

Che-Hsin L, Gwo-Bin L, Bao-Wen C, Guan-Liang C. 2002. A new fabrication process for ultra-thick microfluidic microstructures utilizing SU-8 photoresist. J Micromech Microeng 12:590–597.

Chen CS, Mrksich M, Huang S, Whitesides GM, Ingber DE. 1997. Geometric control of cell life and death. Science 276:1425–1428.

Chen CS, Mrksich M, Huang S, Whitesides GM, Ingber DE. 1998. Micropatterned surfaces for control of cell shape, position, and function. Biotechnol Prog 14:356–363.

Chu VT, Gage FH. 2001. Chipping away at stem cells. Proc Natl Acad Sci U S A 98:7652–7653.

Clark P, Britland S, Connolly P. 1993. Growth cone guidance and neuron morphology on micropatterned laminin surfaces. J Cell Sci 105:203–212.

Denn MM. 1980. Process fluid mechanics. Englewood Cliffs, NJ: Prentice-Hall.

Doetsch F. 2003. A niche for adult neural stem cells. Curr Opin Genet Dev 13:543–550.

Flax JD, Aurora S, Yang C, Simonin C, Wills AM, Billinghurst LL, Jendoubi M, Sidman RL, Wolfe JH, Kim SU et al. 1998. Engraftable human neural stem cells respond to developmental cues, replace neurons, and express foreign genes. Nat Biotechnol 16:1033–1039.

Flynn RA, Birkbeck AL, Gross M, Ozkan M, Shao B, Wang MM, Esener SC. 2002. Parallel transport of biological cells using individually addressable VCSEL arrays as optical tweezers. Sensors Actuators B-Chem 87:239–243.

Francis K, Palsson BO. 1997. Effective intercellular communication distances are determined by the relative time constants for cyto/chemokine secretion and diffusion. Proc Natl Acad Sci U S A 94:12258–12262.

Freshney RI. 2000. Culture of animal cells: a manual of basic technique. New York: John Wiley & Sons.

Gage FH, Coates PW, Palmer TD, Kuhn HG, Fisher LJ, Suhonen JO, Peterson DA, Suhr ST, Ray J. 1995a. Survival and differentiation of adult neuronal progenitor cells transplanted to the adult brain. Proc Natl Acad Sci U S A 92:11879–11883.

Gage FH, Ray J, Fisher LJ. 1995b. Isolation, characterization, and use of stem cells from the CNS. Annu Rev Neurosci 18:159–192.

Haberman R. 1998. Elementary applied partial differential equations: with Fourier series and boundary value problems. Upper Saddle River, NJ: Prentice Hall.

Hammarback JA, McCarthy JB, Palm SL, Furcht LT, Letourneau PC. 1988. Growth cone guidance by substrate-bound laminin pathways is correlated with neuron-to-pathway adhesivity. Dev Biol 126:29–39.

Heuschkel MO, Guerin L, Buisson B, Bertrand D, Renaud P. 1998. Buried microchannels in photopolymer for delivering of solutions to neurons in a network. Sensors Actuators B-Chem 48:356–361.

Hugnot JP, Mellodew K, Pilcher H, Uwanogho D, Price J, Sinden JD. 2001. Direct cell-cell interactions control apoptosis and oligodendrocyte marker expression of neuroepithelial cells. J Neurosci Res 65: 195–207.

Inoue I, Wakamoto Y, Moriguchi H, Okano K, Yasuda K. 2001. On-chip culture system for observation of isolated individual cells. Lab on a Chip 1:50–55.

Ivanova NB, Dimos JT, Schaniel C, Hackney JA, Moore KA, Lemischka IR. 2002. A stem cell molecular signature. Science 298:601–604.

Jackman RJ, Duffy DC, Ostuni E, Willmore ND, Whitesides GM. 1998. Fabricating large arrays of microwells with arbitrary dimensions and filling them using discontinuous dewetting. Anal Chem 70:2280–2287.

Jacquez JA. 1972. Compartmental analysis in biology and medicine. Kinetics of distribution of tracer-labeled materials. Amsterdam: Elsevier.

Kalcheim C, Carmeli C, Rosenthal A. 1992. Neurotrophin 3 is a mitogen for cultured neural crest cells. Proc Natl Acad Sci U S A 89:1661–1665.

Kallos MS, Behie LA. 1999. Inoculation and growth conditions for high-cell-density expansion of mammalian neural stem cells in suspension bioreactors. Biotechnol Bioeng 63:473–483.

Krevelen DWv. 1990. Properties of polymers: their correlation with chemical structure, their numerical estimation and prediction from additive group contributions. Amsterdam: Elsevier.

Lai K, Kaspar BK, Gage FH, Schaffer DV. 2003. Sonic hedgehog regulates adult neural progenitor proliferation in vitro and in vivo. Nat Neurosci 6:21–27.

Lemischka I. 1999. Searching for stem cell regulatory molecules. Some general thoughts and possible approaches. Ann N Y Acad Sci 872: 274–287; discussion 287–288.

Li Jeon N, Baskaran H, Dertinger SK, Whitesides GM, Van de Water L, Toner M. 2002. Neutrophil chemotaxis in linear and complex gradients of interleukin-8 formed in a microfabricated device. Nat Biotechnol 20:826–830.

Lodin Z, Booher J, Kasten FH. 1970. Phase-contrast cinematographic study of dissociated neurons from embryonic chick dorsal root ganglia cultured in the rose chamber. Exp Cell Res 60:27–39.

Lois C, Alvarez-Buylla A. 1993. Proliferating subventricular zone cells in the adult mammalian forebrain can differentiate into neurons and glia. Proc Natl Acad Sci U S A 90:2074–2077.

MacBeath G, Schreiber SL. 2000. Printing proteins as microarrays for high-throughput function determination. Science 289:1760–1763.

Morrison SJ, Shah NM, Anderson DJ. 1997. Regulatory mechanisms in stem cell biology. Cell 88:287–298.

Nakauchi H, Sudo K, Ema H. 2001. Quantitative assessment of the stem cell self-renewal capacity. Ann N Y Acad Sci 938:18–24; discussion 24–25.

Nelson CM, Chen CS. 2002. Cell-cell signaling by direct contact increases cell proliferation via a PI3K-dependent signal. FEBS Lett 514: 238–242.

Nelson CM, Raghavan S, Tan JL, Chen CS. 2003. Degradation of micropatterned surfaces by cell-dependent and -independent processes. Langmuir 19:1493–1499.

Orfao A, Ruiz-Arguelles A. 1996. General concepts about cell sorting techniques. Clin Biochem 29:5–9.

Ostuni E, Chen CS, Ingber DE, Whitesides GM. 2001. Selective deposition of proteins and cells in arrays of microwells. Langmuir 17: 2828–2834.

Ozkan M, Pisanic T, Scheel J, Barlow C, Esener S, Bhatia SN. 2003. Electro-optical platform for the manipulation of live cells. Langmuir 19:1532–1538.

Palmer TD, Markakis EA, Willhoite AR, Safar F, Gage FH. 1999. Fibroblast growth factor-2 activates a latent neurogenic program in neural stem cells from diverse regions of the adult CNS. J Neurosci 19: 8487–8497.

Palsson BO, Koller MR, Eisfeld TM. Oncosis (San Diego, CA), assignee. 2003. Method and apparatus for selectively targeting specific cells within a cell population. USA patent 6,514,722.

Parce JW, Owicki JC, Kercso KM, Sigal GB, Wada HG, Muir VC, Bousse LJ, Ross KL, Sikic BI, McConnell HM. 1989. Detection of cell-affecting agents with a silicon biosensor. Science 246:243–247.

Pease AC, Solas D, Sullivan EJ, Cronin MT, Holmes CP, Fodor SP. 1994. Light-generated oligonucleotide arrays for rapid DNA sequence analysis. Proc Natl Acad Sci U S A 91:5022–5026.

Powers MJ, Domansky K, Kaazempur-Mofrad MR, Kalezi A, Capitano A, Upadhyaya A, Kurzawski P, Wack KE, Stolz DB, Kamm R et al. 2002. A microfabricated array bioreactor for perfused 3D liver culture. Biotechnol Bioeng 78:257–269.

Price JH, Goodacre A, Hahn K, Hodgson L, Hunter EA, Krajewski S, Murphy RF, Rabinovich A, Reed JC, Heynen S. 2002. Advances in molecular labeling, high throughput imaging and machine intelligence portend powerful functional cellular biochemistry tools. J Cell Biochem Suppl 39:194–210.

Ray J, Peterson DA, Schinstine M, Gage FH. 1993. Proliferation, differentiation, and long-term culture of primary hippocampal neurons. Proc Natl Acad Sci U S A 90:3602–3606.

Seetharaman S, Zivarts M, Sudarsan N, Breaker RR. 2001. Immobilized RNA switches for the analysis of complex chemical and biological mixtures. Nat Biotechnol 19:336–341.

Sommer L, Rao M. 2002. Neural stem cells and regulation of cell number. Prog Neurobiol 66:1–18.

Song H, Stevens CF, Gage FH. 2002. Astroglia induce neurogenesis from adult neural stem cells. Nature 417:39–44.

Suslov ON, Kukekov VG, Ignatova TN, Steindler DA. 2002. Neural stem cell heterogeneity demonstrated by molecular phenotyping of clonal neurospheres. Proc Natl Acad Sci U S A 99:14506–14511.

Takahashi J, Palmer TD, Gage FH. 1999. Retinoic acid and neurotrophins collaborate to regulate neurogenesis in adult-derived neural stem cell cultures. J Neurobiol 38:65–81.

Taupin P, Ray J, Fischer WH, Suhr ST, Hakansson K, Grubb A, Gage FH. 2000. FGF-2-responsive neural stem cell proliferation requires CCg, a novel autocrine/paracrine cofactor. Neuron 28:385–397.

Taylor LC, Walt DR. 2000. Application of high-density optical microwell arrays in a live-cell biosensing system. Anal Biochem 278:132–142.

Torrance CJ, Agrawal V, Vogelstein B, Kinzler KW. 2001. Use of isogenic human cancer cells for high-throughput screening and drug discovery. Nat Biotechnol 19:940–945.

Tsai RY, McKay RD. 2000. Cell contact regulates fate choice by cortical stem cells. J Neurosci 20:3725–3735.

van Heyningen P, Calver AR, Richardson WD. 2001. Control of progenitor cell number by mitogen supply and demand. Curr Biol 11: 232–241.

Voldman J, Gray ML, Schmidt MA. 1999. Microfabrication in biology and medicine. Annu Rev Biomed Eng 1:401–425.

Voldman J, Gray ML, Toner M, Schmidt MA. 2002. A microfabrication-based dynamic array cytometer. Anal Chem 74:3984–3990.

Voskerician G, Shive MS, Shawgo RS, von Recum H, Anderson JM, Cima MJ, Langer R. 2003. Biocompatibility and biofouling of MEMS drug delivery devices. Biomaterials 24:1959–1967.

Wakamoto Y, Inoue I, Moriguchi H, Yasuda K. 2001. Analysis of single-cell differences by use of an on-chip microculture system and optical trapping. Fresenius J Anal Chem 371:276–281.

Walt DR. 2002. Imaging optical sensor arrays. Curr Opin Chem Biol 6: 689–695.

Wu RZ, Bailey SN, Sabatini DM. 2002. Cell-biological applications of transfected-cell microarrays. Trends Cell Biol 12:485–488.

Yaworsky PJ, Kappen C. 1999. Heterogeneity of neural progenitor cells revealed by enhancers in the nestin gene. Dev Biol 205:309–321.

You AJ, Jackman RJ, Whitesides GM, Schreiber SL. 1997. A miniaturized arrayed assay format for detecting small molecule-protein interactions in cells. Chem Biol 4:969–975.

Young ME, Carroad PA, Bell RL. 1980. Estimation of diffusion coefficients of proteins. Biotechnol Bioeng 22:947–955.

Ziauddin J, Sabatini DM. 2001. Microarrays of cells expressing defined cDNAs. Nature 411:107–110.